RSC Advances

PAPER

View Article Online
View Journal | View Issue

Cite this: *RSC Adv.*, 2017, **7**, 22400

Green synthesis of luminescent and defect-free bio-nanosheets of MoS_2: interfacing two-dimensional crystals with hydrophobins†

Jasneet Kaur, ‡[a] Alfredo Maria Gravagnuolo, ‡§*[b] Pasqualino Maddalena,[a] Carlo Altucci,[a] Paola Giardina [b] and Felice Gesuele *[a]

Received 9th February 2017
Accepted 13th April 2017

DOI: 10.1039/c7ra01680h

rsc.li/rsc-advances

Solution processing and biofunctionalization of two-dimensional crystals are pivotal for their (biomedical) applications. Here we interface ultrathin layers of MoS_2 with the surface active and self-assembling fungal proteins named Vmh2, which belong to the hydrophobin family. We produce few-layered biofunctionalized MoS_2 (bio-MoS_2) nanosheets *via* liquid phase exfoliation in a green solvent, and controlled centrifugation; a low-cost and eco-friendly process. The dispersions are investigated by electrophoretic mobility, atomic force microscopy (AFM), UV-Vis, Raman and photoluminescence (PL) spectroscopy. The nanosheets present a defect-free vibrational spectrum, tunable zeta-potential and their photoluminescence is preserved after non-covalent biofunctionalization making them well suited for various biomedical applications.

Introduction

Over the last decade, the isolation of single atomic layers of graphene has sparked intense activity in two-dimensional (2D) layered materials research due to their unprecedented quantum and physicochemical properties.[1,2] Starting from graphene, which is a semi-metal, the study of layered materials has expanded to 2D alternatives, which exhibit diverse behaviour, including metals, semiconductors, insulators or superconductors, enabling a broad range of applications.[3,4]

Amongst them, semiconducting 2D transition metal dichalcogenides (TMDs) such as MoS_2 have become the primary focus of many researchers.[5] As a matter of fact, monolayer MoS_2 is a direct band gap (about 1.85 eV for the A-exciton transition) semiconductor, while bilayer and few-layer MoS_2 possess smaller indirect band gap.[6] As a consequence a monolayer of MoS_2 exhibits enhancement of the photoluminescence (PL) quantum yield,[7] increased optical non-linearities,[8] strong optical absorption (up to 10%) and excitonic effects at room temperature.[9] The origin of these properties are ascribed to the quantum confinement and dimensionality effects resulting in a modification of the band structure with the varying thickness.[10] MoS_2 nanosheets can also serve as building blocks for the realization of functional hybrid structures where different materials can be assembled in a tailored sequence with novel functionalities.[11,12] Due to their remarkable properties, MoS_2 and its hybrid systems are suitable candidates for the realization of novel optoelectronic, electrochemical, memory and sensing devices.[13–18]

Recent reports also suggest the promising applications of 2D materials in biomedicine ranging from multimodal therapeutics with non-invasive diagnostic capabilities to biosensing and tissue engineering.[19] These prospects push the vast areas of research to put efforts on developing new routes for the synthesis of 2D materials based bio-hybrid systems.[2,20–23]

Since these materials are extremely sensitive to the chemical and physical environment and to the chemical modifications, thus the route for the synthesis and functionalization deeply influences their most relevant properties, either due to the change of the crystalline phase (thin-layered pristine 2H–MoS_2 is a semiconductor, whereas the metastable 1T polytype has metallic nature)[24–26] or to structural defects.[27] The liquid phase exfoliation of layered materials is a versatile top-down strategy for the large scale production of high quality thin sheets starting from the raw and low-cost bulk materials.[28–31]

Two parameters are critical for the characteristics of the solution processed MoS_2. Firstly, the solvent which assists the exfoliation influences the structural quality, toxicity and the stability of the obtained dispersions, among other properties.[21,32,33] In the long-term, the research on the large scale liquid phase exfoliation techniques which encompass the use of green solvents and minimize environmental risk and bio-toxicity, will

[a]*Department of Physics "Ettore Pancini", University of Naples "Federico II", Naples, Italy. E-mail: gesuele@fisica.unina.it*

[b]*Department of Chemical Sciences, University of Naples "Federico II", Naples, Italy. E-mail: alfredomaria.gravagnuolo@unina.it*

† Electronic supplementary information (ESI) available. See DOI: 10.1039/c7ra01680h

‡ The two authors contributed equally to the work.

§ Faculty of Biology, Medicine and Health, The University of Manchester, UK; E-mail: alfredo.gravagnuolo@manchester.ac.uk.

boost the manufacturing, development and biomedical applications of 2D materials.[2,34,35]

Secondly, surface modification can influence the colloidal behaviour of MoS_2, specific interactions with its surroundings, the photoluminescence,[26,36] conductivity and reactivity,[37,38] tailoring its properties to specific environments and applications, in some cases enabling the development of passivation schemes needed to preserve the chemical structure from degradation.[39]

The modification by covalent approaches results in a stable grafting of functionalities, however pristine 2H–MoS_2 is very challenging to functionalize due to its relative inertness and harsh functionalization procedures lead to significant structural changes.[38,40] Conversely, the non-covalent approaches generally preserve the structure of the material with minor modification of the vibrational and electronic properties and is generally less stable.

The functionalization by non-covalent conjugation using biomolecules can be advantageous to create multifunctional complexes for biotechnological applications.[19,41] In addition, interfacing MoS_2 with proteins can improve its biocompatibility and dispersibility as recently reported.[22,42]

Proteins known as the hydrophobins (HFBs) and their engineered variants are quite interesting biomolecules for surface modification, and have been also proven effective for graphene functionalization.[30,43,44] HFBs are compact (around 3 nm linear size) and adhesive cysteine rich proteins endowed with peculiar structural and functional features, produced by fungi.[45] Due to their high amphiphilic character, they are able to self-assemble at hydrophobic/hydrophilic interfaces into ordered monolayers. In their soluble form they show astonishingly high surface activity, indicated by the reduction of the surface tension of water and by a powerful emulsification capacity.[46,47] Moreover, upon adhesion onto various materials they can form nanostructured coatings,[48] able to revert the polarity of the surfaces, to mediate the non-covalent immobilization of a second layer of proteins, peptides and nanomaterials,[49,50] and to improve the stability and the biocompatibility of surfaces.[51,52]

Class I HFBs are able to form chemically stable coatings composed of amyloid-like assemblies, named rodlets, which can be immunologically inert making them of great interest for the stable non-covalent functionalization of biomedical devices and nanodrugs.[48,53] The Class I HFB, Vmh2 is extracted from the mycelium of the edible basidiomycete fungus, *Pleurotus ostreatus*, commonly known as the oyster mushroom.[54] We have recently employed Vmh2 for the one step fabrication of defect-free bio-graphene resulting in stable liquid dispersions.[30] It has been verified that the bio-hybrid complexes are endowed with the self-assembling properties of Vmh2.

The ability of proteins to bind MoS_2 and other nanomaterials can be explained by the presence of a wide assortment of functional groups that can bind to their surface.[49] Guan and coworkers have exploited the density functional theory to simulate the binding energy of the functional groups of a protein, *i.e.* the Bovine Serum Albumin, to MoS_2. They have demonstrated that since the binding energy of some functional groups of the protein is higher than that of an adjacent MoS_2 sheet, therefore the protein can assist the process of liquid phase exfoliation. Interestingly, the structure of Vmh2 presents many of these functional groups, in particular it is rich in disulphide bonds and presents a benzene ring as well as several carboxyl, amino and hydroxyl groups (UniProt Accession Number Q8WZI2; protein chain 25-111).[55] However the interaction of proteins with MoS_2 are still under investigation.[56]

Herein we test Vmh2 for the production of biofunctionalized MoS_2 (bio-MoS_2) nanosheets by an environmental friendly process. The bulk MoS_2 is initially exfoliated in the liquid phase using ultrasonic waves and then non-covalently functionalized with Vmh2. In order to produce dispersions enriched in monolayer content, we exploit the technique of controlled centrifugation.[30] The produced dispersions are therefore, investigated by means of UV-Vis, Raman and photoluminescence (PL) spectroscopy, atomic force microscopy (AFM) and electrophoretic mobility to characterize the most relevant properties of the produced bio-hybrid material.

Results and discussion

Synthesis and dispersion stability of biofunctionalized MoS_2

MoS_2 powder, in 60% ethanol aqueous solution (5 mg in 6.25 mL), was exfoliated for 90 minutes using a tip sonicator at 40 W. The volume of the solvent, the amount of starting material, the shape of the vessel and of the probe, along with the applied power are the crucial parameters in the liquid-phase exfoliation process *via* probe-type (commonly a tip, also named sonotrode) ultrasonic device. Indeed, the acoustic energy is focused on the surface of the probe, and the ultrasonic intensity is a function of the energy input and the sonotrode surface area, however, it rapidly decreases both radially and axially creating dead sonication zones when high volumes are sonicated. For this reason, the distance between the ultrasonic probe and the wall of the vessel must be kept to a minimum.[57] The shape and size of the vessel also affect the solution mixing induced by the sonication, hence, the effectiveness and the reproducibility of the process. Further experimental details of the process are provided in the ESI.†

The obtained dispersion was mixed 10 min by a bath sonicator in aliquots at a variable final concentration of Vmh2, 0 ÷ 75 μg mL^{-1}, and a fixed concentration of MoS_2, 200 μg mL^{-1}, and left for sedimentation.

The colloidal stability of MoS_2 sheets in function of time and Vmh2 concentration is displayed in Fig. 1.

In the absence of Vmh2 the sample was stable over 3 weeks, while at very low concentration of Vmh2, a quick formation of aggregates and precipitation occurred as observed to the naked eye. When the concentration of Vmh2 increased, the stability of the dispersion was gradually improved up to 25 μg mL^{-1}. In order to assess the interaction between Vmh2 and the exfoliated MoS_2, electrophoretic mobility analysis was performed allowing the estimation of the ζ-potential to infer on the surface charge density of the flakes, Fig. 1b.[30,58] The results showed that the charge of the sheets was negative upon exfoliation and gradually changed towards positive values when the protein concentration increased, indicating that Vmh2 molecules, which are

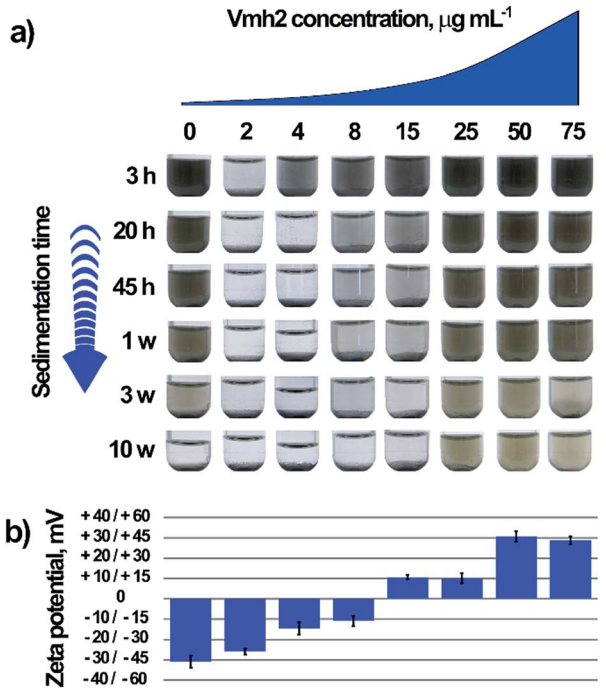

Fig. 1 Dispersion stability of the exfoliated MoS_2 samples. (a) Time stability of the samples dependent on the concentration of Vmh2. (b) Estimated ζ-potential of the MoS_2 samples shown in (a).

positively charged,[30] are able to coat the surface of the flakes reaching the saturation at 50 μg mL^{-1} Vmh2.

We observed that the sheets endowed with high surface charge density, *i.e.* $|\zeta| > 30$ mV obtained using 0, 50 or 75 μg mL^{-1} Vmh2, were stable at least over three weeks. However, the sample at 25 μg mL^{-1} of Vmh2 was very stable even if the value of ζ was too low to justify its stability and the sample at 2 μg mL^{-1} quickly aggregated even if the ζ potential was too high to justify its instability. Additionally, it was possible to observe a very different morphology of aggregates by varying the concentration of Vmh2 (Fig. S1†).

The ζ-potential characterization is commonly used to forecast the stability of liquid dispersions assuming that the electrostatic stabilization plays a fundamental role although it is known that also other factors affect the aggregation/stabilization of nanoparticles such as the steric stabilization by the surfactant[59] and particularly in the case of 2D materials the dynamic interactions among sheets.[60]

The colloidal stability of sheets of graphene from low to high concentrations of a surfactant, *i.e.* sodium dodecyl sulphate from 1.4 to 2880 μg mL^{-1}, has been previously studied by Hsieh and colleagues.[60] They have demonstrated that at the critical concentration of surfactant in which the energy of aggregation and deaggregation of graphene are equal, very compact aggregates and a remarkable reduction of the material concentration in the dispersion are observed. This phenomenon could be explained by the dynamic assembly and disassembly of 2D sheets which results in gradual maximization of the overlap area between sheets leading to different morphologies of aggregates at different concentrations of surfactant.

However, the control of the ζ-potential is crucial for the processing of the nanomaterial in the liquid phase and can influence the interactions of nanosheets towards other materials and biomolecules. Moreover, the possibility to tune the ζ-potential can be useful for drug delivery applications.[61]

Eventually we tested the sedimentation process as a scalable strategy for the separation of the thick particles from the thin ones to produce dispersions of few-layer bio-MoS_2. It has been reported that the UV-Vis spectral profile of the MoS_2 dispersions are dependent on the lateral size and thickness of the flakes and this relationship can be expressed by metrics.[10]

Therefore, the supernatant of the dispersion after 15 weeks was analysed by UV-Vis spectroscopy estimating the number of layer per flake as reported by Backes and colleagues (Fig. S2†). Since the mean number of layers determined by UV-Vis analysis was greater than 10, thus in order to obtain thinner flakes, we implemented the protocol with the technique of controlled centrifugation.

Particle size selection

MoS_2 crystals, in 60% ethanol aqueous solution (5 mg in 5 mL), were exfoliated for 2 hours using a tip sonicator 18 W power (see ESI† for details). The nanosheets produced after exfoliation are polydisperse in size and thickness because of the stochastic fragmentation. Therefore, aliquots of the obtained dispersions were serially centrifuged at 40, 150, 600 and 2400*g* for 45 minutes each in the presence of Vmh2 at the concentrations which lie in the stability range, *i.e.* Vmh2 > 25 μg mL^{-1} or in its absence. After every step of centrifugation, large and thick flakes were removed in the form of pellet and the resultant supernatant was proceeded with the next step of centrifugation which makes it more refined in size and thickness. The extinction spectrum in the UV-Vis region of the sample supernatant was acquired after every step of centrifugation, analysed and compared with the previous steps, plotted in Fig. 2.

The extinction spectrum is the sum of contributions from both absorbance and scattering components. However, scattering contribution is more prominent upon centrifugation at 40 and 160*g* than at 600 and 2400*g* as indicated by more intense extinction at ~800 nm.[10]

On analysing the spectra of the dispersions for each step of centrifugation, we estimated the mean number of layers per flake $\langle \bar{N} \rangle$ (Fig. 2b), the mean lateral size $\langle \bar{L} \rangle$ (Fig. 2c) and the concentration of the sample (Fig. S3†) as reported elsewhere (details in ESI†).[10] As the centrifugal force was increased, the A-exciton peak shifted towards lower wavelengths, signifying reduction in number of layers of the flakes and leading to few-layer enriched dispersions (Fig. 2a). Moreover, the B-exciton extinction upon spectrum normalization at 350 nm contains the information on the mean length of the flakes.

At the higher centrifugal force tested, 2400*g*, $\langle \bar{N} \rangle$ was estimated ~2 ÷ 3 layers and $\langle \bar{L} \rangle$ ~100 nm. Moreover, when Vmh2 was used at a concentration lying in the stability range, no significant difference in size was observed among exfoliated samples using different concentrations of the protein (Fig. 2b and c).

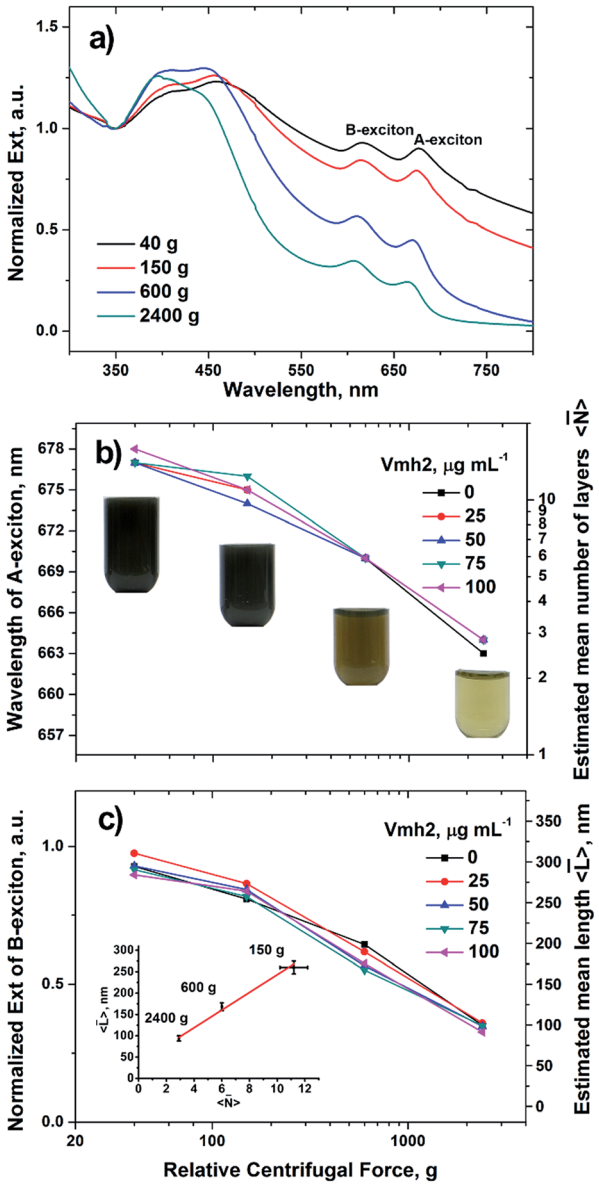

Fig. 2 Controlled centrifugation process for size selection of MoS_2 particles. (a) Extinction spectra normalized at 350 nm of MoS_2 samples exfoliated and mixed with 50 μg mL^{-1} Vmh2, at different steps of centrifugation. (b) Wavelength of A-exciton extracted from spectra shown in (a), corresponding estimated mean number of layers per particle and images of the samples. Effect of Vmh2 concentration in the stability range. (c) Extinction of B-exciton extracted from spectra shown in (a), corresponding estimated lateral size of the particles and comparison with other Vmh2 concentrations in which dispersions are stable. (c-inset) Comparison of mean length and thickness of samples.

We also estimated $\langle \bar{L} \rangle$ through dynamic light scattering (DLS), using the metric reported by Lotya and colleagues.[62] The lateral size were consistent among the UV-Vis and DLS metrics (Table S1†), except than at 25 μg mL^{-1} Vmh2 in which we estimated a slightly higher value of $\langle \bar{L} \rangle$ using DLS. Since the lateral size of the protein is more than one order of magnitude smaller than that of the flakes, its presence on the surface cannot influence the analysis. On the other hand, at this concentration of Vmh2 the dispersions are at the limit of the stability range, therefore, partial MoS_2 aggregation could explain the increase of the apparent lateral size only by DLS and not by UV-Vis analysis.

Furthermore, electrophoretic mobility measurements of the centrifuged samples also exhibited the reversal of ζ-potential of the flakes (from −23 mV to +32 mV) confirming the interaction of the protein with the material (Table S1†).

Nanoscopic characterization

We investigated the distribution of layers of the exfoliated bio-MoS_2 flakes by means of atomic force microscopy[63] and their vibrational and electronic properties by means of Raman[64] and photoluminescence spectroscopy at single particle level.

After the process of size selection by centrifugation, the exfoliated flakes of bio-MoS_2 were deposited onto SOI (silicon dioxide on silicon) substrates by drop-casting, ensuring that the process resulted in a sparse distribution of isolated particles.

We employed an Atomic Force Microscope (Witec Alpha SNOM RAS 300) in intermittent contact mode in order to perturb as less as possible the adhesion of the flakes to the substrate. Several AFM scans allowed to estimate the thickness of a monolayer in the range of 1–1.4 nm, this value being in agreement with others presented in literature both for mechanical exfoliated flakes[65] and liquid phase exfoliated nanosheets.[35,66] For biofunctionalized flakes, there is clearly an offset due to the HFB encapsulation, which strongly depends on the concentration of Vmh2. At higher concentration, we found that the dried flakes were surrounded by several nanometers Vmh2 encapsulation, which prevented us to quantitatively estimate the layer thicknesses. We infer, from the macroscopic absorption and from the micro-Raman (which follows), that the Vmh2 encapsulation does not perturb the inter-layers spacing.

In Fig. 3 we report a characteristic AFM scan on non-encapsulated sample over a relative large area showing large distribution of sizes and area. The topographic analysis summarized in the histogram (Fig. 3b) shows a distribution of layer which can be described, in first approximation by a Poisson distribution, as reported by recent literature.[67]

The average number of layers per flake is in the 3 ÷ 5 range, in good agreement with the estimation based on UV-Vis metric analysis. Monolayer flakes are present in low percentage, and significant percentage of bi-layers and tri-layers appears. The possibility to obtain few-layer flakes including monolayers makes this technique of interest in several fields of research. The monolayer percentage can be further increased with a careful choice of the centrifugation steps and parameters as recently demonstrated for liquid phase exfoliation of TMD in organic solvent.[68]

We employed confocal Raman spectroscopy and imaging both to confirm the presence of monolayers and to investigate the modifications of the vibrational spectrum, which are related to the chemical properties of the bio-functionalized nanosheets. Raman spectroscopy is indeed a widely employed method to estimate the thickness of TMD flakes as well as the presence of defects.[69]

A typical Raman spectrum of MoS_2 shows several characteristic peaks corresponding to in-plane and out-of-plane

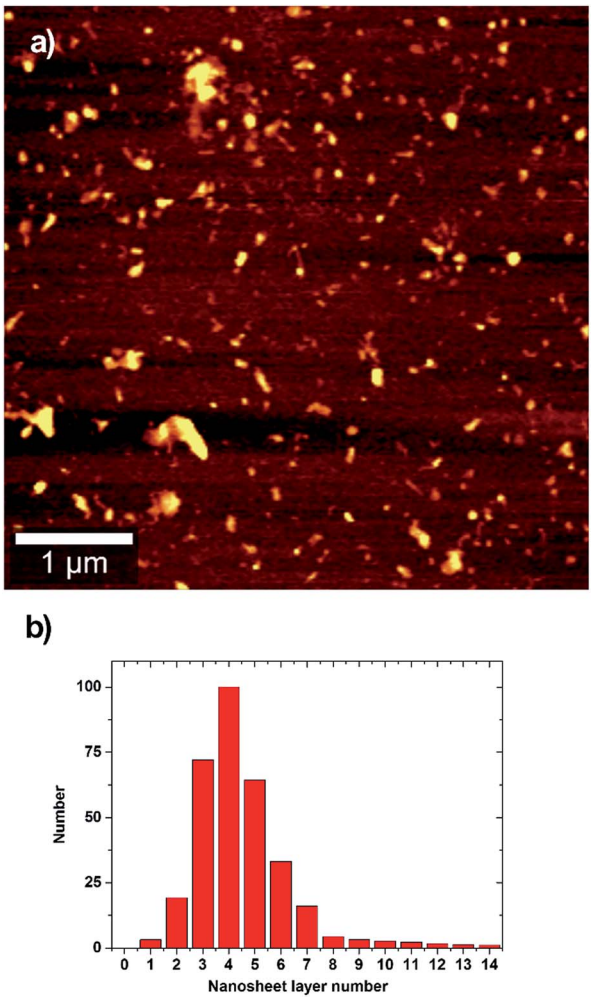

Fig. 3 Atomic force microscopy and height analysis for exfoliated MoS_2. (a) A typical AFM scan of deposited MoS_2 nanosheets. (b) Statistical distribution of the layer number per particle.

vibrational modes. Two peaks at about 380 cm^{-1} and 403 cm^{-1} are widely investigated; they correspond to the in-plane E^1_{2g} and out-of-plane A_{1g} vibrational modes. The change in the layer number results in a modification of the vibrational Raman spectrum of MoS_2.

The E^1_{2g} and A_{1g} modes strongly depend on the modification of bulk structure in the monolayer limit with an increase for the E^1_{2g} resonant frequency and a corresponding decrease of the A_{1g} one. This displacement of the peaks position allows for an identification of the number of layers per flake. Here we employed confocal laser scanning microscopy coupled to Raman spectroscopy at the single particle level.

We set the excitation wavelength at 488 nm, well above the bandgap, to avoid effects of resonant Raman emission[70] which would result in a more complicated Raman spectrum. Moreover, the spatial resolution at this excitation wavelength (about 350 nm) is well below the average separation between flakes, allowing us to image single isolated nanosheets.

In Fig. 4 we report a Raman image on deposited bio-MoS_2 ([Vmh2] = 75 μg mL^{-1}). At every point, an entire spectrum was

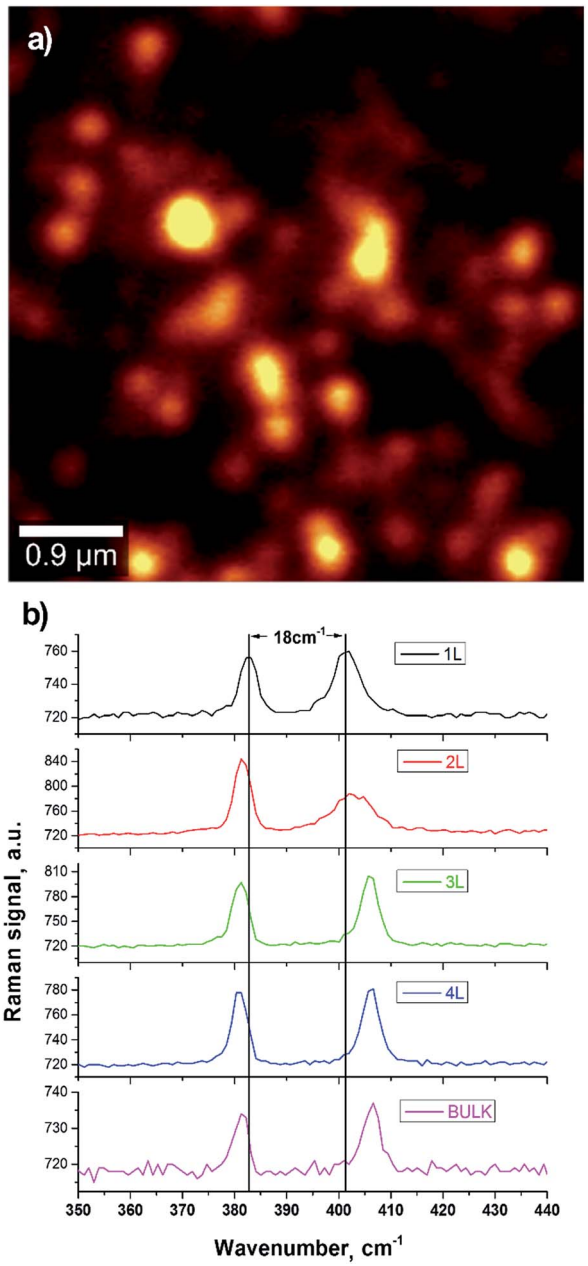

Fig. 4 Raman spectroscopy and imaging over the two main vibrational modes E^1_{2g} and A_{1g}. (a) Imaging the Raman intensity of the E^1_{2g} and A_{1g} vibrational modes of bio-MoS_2; the image represents the integrated Raman signal in the 375–415 cm^{-1} range (b) evolution of Raman spectrum from bulk to monolayer flakes.

collected and the image represents, point by point, the integrated Raman intensity over the spectral region of the two investigated peaks. We observed the presence of nanosheets with Raman spectrum corresponding to that of a monolayer, with a frequency separation of about 18 cm^{-1} in agreement with reported data in literature.[69] This confirmed the possibility to obtain monolayer flakes encapsulated by Vmh2. We observed the modification of the spectrum from flake to flake with a change in the frequency separation of the two main peaks, indicating the presence of 1–4 layers.

The Raman integrated intensity change from flake to flake due to the competition of several effects: with the increase of the number of layers, there is an increase (i) of the Raman nonlinearity and (ii) of the linear absorption at pump and Raman wavelengths; (iii) with the increase of the area there is an overall increase of the Raman signal. The measured Raman spectrum follows that of the 2H–MoS_2 semiconductive phase. This is consistent with the linear macroscopic absorption (*i.e.* the appearance of A and B excitons peaks by UV-Vis spectroscopy, shown in Fig. 2) and excludes the presence of significant amount of 1T metallic phase.[71]

The shape and the width of the resonant peaks are in well agreement with the data reported in literature[69,72] and indicate low defects in the produced MoS_2 nanosheets. These results demonstrate that the non-covalent functionalization by Vmh2 does not modify significantly the vibrational properties of the exfoliated material.

We investigated the electronic properties of bio-MoS_2 at the single particle level. It is well known, as previously mentioned, that in the limit of monolayer the MoS_2 becomes a direct-gap semiconductor with an increase of the photoluminescence emission yield. PL emission may depend on several factors including the dielectric environment, photo-induced chemical reaction and oxidation.[73] Aiming to verify if this behaviour was preserved by the Vmh2 encapsulation, we performed photoluminescence spectroscopy and imaging of single isolated nanosheets. The results are shown in Fig. 5 for a Vmh2 encapsulated sample ([Vmh2] = 75 μg mL^{-1}). We employed the Raman spectroscopy to identify region 1 or 2 or 3 layers thick and measured their PL emission. The results clearly show larger emission from the monolayer flakes with a PL peak at 670 nm (1.85 eV) which corresponds to the A-exciton of the MoS_2 band structures. With the increase of the layer number the PL reduces and a second peak appear at 620 nm (2 eV) corresponding to the B-exciton.

The occurrence of two PL peaks is consequence of the splitting of the valence band due to spin–orbit coupling. This results in the occurrence of the two direct excitonic transitions (A and B-exciton) at the *K*-point of the band structure. Few-layer MoS_2 presents an indirect band-gap with lower energy than the A- and B-gaps. At the monolayer limit, the indirect band-gap becomes larger, while the direct A- and B-transitions change only by a little amount. Interestingly the PL emission from the Vmh2 encapsulated flakes is stable under photoirradiation for minutes preventing effects of photo-oxidation which have been reported in literature[73] for chemical vapour deposition grown and mechanical exfoliated samples. We infer that the Vmh2 non-covalent functionalization preserves the photoluminescence emission of few-layer MoS_2 resulting to be stable against effects of oxygen adsorption and photo-oxidation.

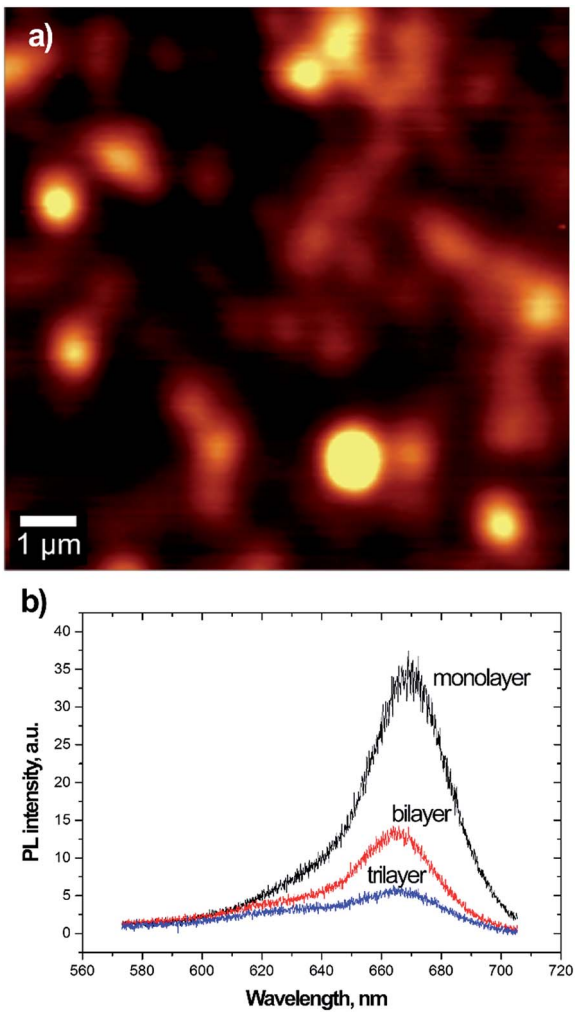

Fig. 5 Photoluminescence spectroscopy and imaging for bio-MoS_2. (a) PL imaging; the image represents the integrate PL signal in the spectral window of 580–710 nm. (b) Evolution of PL signal for one, two and three layers regions as identified by Raman spectroscopy.

Conclusions

We have produced dispersions of few-layered, defect-free, bio-functionalized sheets of 2H–MoS_2, through a green route, interfacing, for the first time, this material with a self-assembling protein, *i.e.* Vmh2, which belongs to the hydrophobin family. The protein which is adsorbed on the surface of the sheets is used to tune their ζ-potential and the colloidal behaviour that is essential for the solution processing of the nanosheets,[74] additionally, the material is photoluminescent and stable in air against photo-oxidation.

By monitoring the Raman and PL emission at the single-particle level, we have demonstrated that the non-covalent functionalization through Vmh2 preserves a defect-free vibrational spectrum of MoS_2 nanosheets. Moreover, their electronic properties resemble that of the pristine material, as verified by the increase of photoluminescence emission in the monolayer limit, which is due to the change from indirect to direct band-gap. Biologically functionalized luminescent nanosheets are of interest for a wide range of applications from bioimaging[75] to optical biosensing.[76]

This technique of preparation of nanosheets is versatile, indeed, it can be easily extended to other 2D materials and conditions (see electronic ESI Fig. S6–S8† for the functionalization of WS_2), inspiring further investigation on the

mechanism of stabilization/aggregation of 2D materials. Moreover, this tool can be extended to the fabrication of polymer nanocomposites, nano-bio-hybrid systems and heterostructures with novel and tailored properties.[11,74,77]

The electronic properties of MoS_2 have been demonstrated[78,79] advantageous in pioneeristic studies on FET based biosensors showing superior performance even when compared to graphene[80] and when it has been bioconjugated with proteinaceous receptors to increase the sensor selectivity.[81] Scalable production of FET-protein hybrids will enable their industrial exploitation.[82] Additionally, the availability of controllable modification strategies for MoS_2 surface could generate tunable electronic and structural properties, which would be of great significance for potential nanoscale applications and flexible electronics.[83–85]

In conclusion, we expect that this biofunctionalized material will be useful for (nano)biomedical applications and, since the process of production is inherently scalable, it will offer the prospect of a significant boost of the use of bio-MoS_2 in these fields.[2,17,19,42,86]

Acknowledgements

This work was partially supported by the Italian Ministry for University and Research within the framework of the Operative National Programme PON 2007–2013, through Project "CeSMA" (Centro di Servizi di Misure Avanzate, Asse I, Obiettivo Operativo 4.1.1.4) and the Industrial research project "BioPoliS" (Development of green technologies for the production of BIOchemicals and their use in the preparation and industrial application of POLImeric materials from agricultural biomasses cultivated in a sustainable way in the Campania region, PON03PE_00107_1, D. D. Prot. N. 713/Ric. 29/10/2010). Moreover the work was supported through the project IENA ("Immobilization of Enzymes on hydrophobin-functionalized NAnomaterials") within the framework of the University research program "Programma per il finanziamento della ricerca di Ateneo" D. R. n. 409 7/02/2017. The authors would like to thank Prof. Gennaro Marino for his helpful advice.

References

1 K. S. Novoselov, D. Jiang, F. Schedin, T. J. Booth, V. V. Khotkevich, S. V Morozov and A. K. Geim, *Proc. Natl. Acad. Sci. U. S. A.*, 2005, **102**, 10451–10453.

2 A. C. Ferrari, F. Bonaccorso, V. Fal'ko, K. S. Novoselov, S. Roche, P. Bøggild, S. Borini, F. H. L. Koppens, V. Palermo, N. Pugno, J. A. Garrido, R. Sordan, A. Bianco, L. Ballerini, M. Prato, E. Lidorikis, J. Kivioja, C. Marinelli, T. Ryhänen, A. Morpurgo, J. N. Coleman, V. Nicolosi, L. Colombo, A. Fert, M. Garcia-Hernandez, A. Bachtold, G. F. Schneider, F. Guinea, C. Dekker, M. Barbone, Z. Sun, C. Galiotis, A. N. Grigorenko, G. Konstantatos, A. Kis, M. Katsnelson, L. Vandersypen, A. Loiseau, V. Morandi, D. Neumaier, E. Treossi, V. Pellegrini, M. Polini, A. Tredicucci, G. M. Williams, B. H. Hong, J.-H. Ahn, J. M. Kim, H. Zirath, B. J. van Wees, H. van der Zant, L. Occhipinti, A. Di Matteo, I. A. Kinloch, T. Seyller, E. Quesnel, X. Feng, K. Teo, N. Rupesinghe, P. Hakonen, S. R. T. Neil, Q. Tannock, T. Löfwander and J. Kinaret, *Nanoscale*, 2015, **7**, 4598–4810.

3 Y. Chen, B. Zhang, G. Liu, X. Zhuang and E.-T. Kang, *Chem. Soc. Rev.*, 2012, **41**, 4688–4707.

4 R. F. Service, *Science*, 2015, **348**, 490–492.

5 M. Xu, T. Liang, M. Shi and H. Chen, *Chem. Rev.*, 2013, **113**, 3766–3798.

6 A. Splendiani, L. Sun, Y. Zhang, T. Li, J. Kim, C.-Y. Chim, G. Galli and F. Wang, *Nano Lett.*, 2010, **10**, 1271–1275.

7 K. F. Mak, C. Lee, J. Hone, J. Shan and T. F. Heinz, *Phys. Rev. Lett.*, 2010, **105**, 136805.

8 Y. Li, Y. Rao, K. F. Mak, Y. You, S. Wang, C. R. Dean and T. F. Heinz, *Nano Lett.*, 2013, **13**, 3329–3333.

9 Y. You, X.-X. Zhang, T. C. Berkelbach, M. S. Hybertsen, D. R. Reichman and T. F. Heinz, *Nat. Phys.*, 2015, **11**, 477–481.

10 C. Backes, R. J. Smith, N. McEvoy, N. C. Berner, D. McCloskey, H. C. Nerl, A. O'Neill, P. J. King, T. Higgins, D. Hanlon, N. Scheuschner, J. Maultzsch, L. Houben, G. S. Duesberg, J. F. Donegan, V. Nicolosi and J. N. Coleman, *Nat. Commun.*, 2014, **5**, 4576.

11 A. K. Geim and I. V. Grigorieva, *Nature*, 2013, **499**, 419–425.

12 O. A. Ajayi, N. C. Anderson, M. Cotlet, N. Petrone, T. Gu, A. Wolcott, F. Gesuele, J. Hone, J. S. Owen and C. W. Wong, *Appl. Phys. Lett.*, 2014, **104**, 171101.

13 G. R. Bhimanapati, Z. Lin, V. Meunier, Y. Jung, J. Cha, S. Das, D. Xiao, Y. Son, M. S. Strano, V. R. Cooper, L. Liang, S. G. Louie, E. Ringe, W. Zhou, S. S. Kim, R. R. Naik, B. G. Sumpter, H. Terrones, F. Xia, Y. Wang, J. Zhu, D. Akinwande, N. Alem, J. A. Schuller, R. E. Schaak, M. Terrones and J. A. Robinson, *ACS Nano*, 2015, **9**, 11509–11539.

14 F. Gesuele, S. Lettieri, P. Maddalena, M. Liscidini and L. C. Andreani, *J. Phys. B: At., Mol. Opt. Phys.*, 2007, **40**, 727–734.

15 X. Liu, T. Galfsky, Z. Sun, F. Xia and E. Lin, *Nat. Photonics*, 2015, **9**, 30–34.

16 E. Descrovi, C. Ricciardi, F. Giorgis, G. Lérondel, S. Blaize, C. X. Pang, R. Bachelot, P. Royer, S. Lettieri, F. Gesuele, P. Maddalena and M. Liscidini, *Opt. Express*, 2007, **15**, 4159–4167.

17 D. Jariwala, V. K. Sangwan, L. J. Lauhon, T. J. Marks and M. C. Hersam, *ACS Nano*, 2014, **8**, 1102–1120.

18 C. Tan, Z. Liu, W. Huang and H. Zhang, *Chem. Soc. Rev.*, 2015, **44**, 2615–2628.

19 R. Kurapati, K. Kostarelos, M. Prato and A. Bianco, *Adv. Mater.*, 2016, **28**, 6052–6074.

20 W. Zhang, P. Zhang, Z. Su and G. Wei, *Nanoscale*, 2015, **7**, 18364–18378.

21 W. Zhang, Y. Wang, D. Zhang, S. Yu, W. Zhu, J. Wang, F. Zheng, S. Wang and J. Wang, *Nanoscale*, 2015, **7**, 10210–10217.

22 G. Guan, S. Zhang, S. Liu, Y. Cai, M. Low, C. P. Teng, I. Y. Phang, Y. Cheng, K. L. Duei, B. M. Srinivasan, Y. Zheng, Y. W. Zhang and M. Y. Han, *J. Am. Chem. Soc.*, 2015, **137**, 6152–6155.

23 M. Ayán-Varela, Ó. Pérez-Vidal, J. I. Paredes, J. M. Munuera, S. Villar-Rodil, M. Díaz-González, C. Fernández-Sánchez, V. S. Silva, M. Cicuéndez, M. Vila, A. Martínez-Alonso and J. M. D. Tascón, *ACS Appl. Mater. Interfaces*, 2017, **9**, 2835–2845.
24 D. Voiry, A. Goswami, R. Kappera, C. d. C. C. e. Silva, D. Kaplan, T. Fujita, M. Chen, T. Asefa and M. Chhowalla, *Nat. Chem.*, 2015, **7**, 45–49.
25 Y.-C. Lin, D. O. Dumcenco, Y.-S. Huang and K. Suenaga, *Nat. Nanotechnol.*, 2014, **9**, 391–396.
26 G. Eda, H. Yamaguchi, D. Voiry, T. Fujita, M. Chen and M. Chhowalla, *Nano Lett.*, 2011, **11**, 5111–5116.
27 Z. Lin, B. R. Carvalho, E. Kahn, R. Lv, R. Rao, H. Terrones, M. A. Pimenta and M. Terrones, *2D Mater.*, 2016, **3**, 22002.
28 E. Varrla, C. Backes, K. R. Paton, A. Harvey, Z. Gholamvand, J. McCauley and J. N. Coleman, *Chem. Mater.*, 2015, **27**, 1129–1139.
29 L. Niu, J. N. Coleman, H. Zhang, H. Shin, M. Chhowalla and Z. Zheng, *Small*, 2016, **12**, 272–293.
30 A. M. Gravagnuolo, E. Morales-Narváez, S. Longobardi, E. T. Da Silva, P. Giardina and A. Merkoçi, *Adv. Funct. Mater.*, 2015, **25**, 2771–2779.
31 C. Backes, T. M. Higgins, A. Kelly, C. Boland, A. Harvey, D. Hanlon and J. N. Coleman, *Chem. Mater.*, 2017, **29**, 243–255.
32 J. Choi, H. Zhang, H. Du and J. H. Choi, *ACS Appl. Mater. Interfaces*, 2016, **8**, 8864–8869.
33 J. Shen, Y. He, J. Wu, C. Gao, K. Keyshar, X. Zhang, Y. Yang, M. Ye, R. Vajtai, J. Lou and P. M. Ajayan, *Nano Lett.*, 2015, **15**, 5449–5454.
34 A. Bianco and M. Prato, *2D Mater.*, 2015, **2**, 30201.
35 Y. Qi, N. Wang, Q. Xu, H. Li, P. Zhou, X. Lu and G. Zhao, *Chem. Commun.*, 2015, **51**, 6726–6729.
36 M. Amani, D.-H. Lien, D. Kiriya, J. Xiao, A. Azcatl, J. Noh, S. R. Madhvapathy, R. Addou, S. Kc, M. Dubey, K. Cho, R. M. Wallace, S.-C. Lee, J.-H. He, J. W. Ager, X. Zhang, E. Yablonovitch and A. Javey, *Science*, 2015, **350**, 1065–1068.
37 S. Presolski and M. Pumera, *Mater. Today*, 2016, **19**, 140–145.
38 C. Backes, N. C. Berner, X. Chen, P. Lafargue, P. LaPlace, M. Freeley, G. S. Duesberg, J. N. Coleman and A. R. McDonald, *Angew. Chem., Int. Ed. Engl.*, 2015, **54**, 2638–2642.
39 C. R. Ryder, J. D. Wood, S. A. Wells and M. C. Hersam, *ACS Nano*, 2016, **10**, 3900–3917.
40 X. Chen, N. C. Berner, C. Backes, G. S. Duesberg and A. R. McDonald, *Angew. Chem., Int. Ed.*, 2016, **55**, 5803–5808.
41 J. I. Paredes and S. Villar-Rodil, *Nanoscale*, 2016, **8**, 15389–15413.
42 R. Deng, H. Yi, F. Fan, L. Fu, Y. Zeng, Y. Wang, Y. Li, Y. Liu, S. Ji and Y. Su, *RSC Adv.*, 2016, **6**, 77083–77092.
43 K. Scholtmeijer, M. I. Janssen, B. Gerssen, M. L. de Vocht, B. M. van Leeuwen, T. G. van Kooten, H. a B. Wösten and J. G. H. Wessels, *Appl. Environ. Microbiol.*, 2002, **68**, 1367–1373.
44 P. Laaksonen, M. Kainlauri, T. Laaksonen, A. Shchepetov, H. Jiang, J. Ahopelto and M. B. Linder, *Angew. Chem., Int. Ed.*, 2010, **49**, 4946–4949.
45 J. Bayry, V. Aimanianda, J. I. Guijarro, M. Sunde and J.-P. Latgé, *PLoS Pathog.*, 2012, **8**, e1002700.
46 W. Wohlleben, T. Subkowski, C. Bollschweiler, B. von Vacano, Y. Liu, W. Schrepp and U. Baus, *Eur. Biophys. J.*, 2010, **39**, 457–468.
47 P. Cicatiello, A. M. Gravagnuolo, G. Gnavi, G. C. Varese and P. Giardina, *Int. J. Biol. Macromol.*, 2016, **92**, 1229–1233.
48 V. Lo, Q. Ren, C. Pham, V. Morris, A. Kwan and M. Sunde, *Nanomaterials*, 2014, **4**, 827–843.
49 A. M. Gravagnuolo, E. Morales-Narváez, C. R. S. Matos, S. Longobardi, P. Giardina and A. Merkoçi, *Adv. Funct. Mater.*, 2015, **25**, 6084–6092.
50 S. Longobardi, A. M. Gravagnuolo, R. Funari, B. Della Ventura, F. Pane, E. Galano, A. Amoresano, G. Marino and P. Giardina, *Anal. Bioanal. Chem.*, 2015, **407**, 487–496.
51 H. A. B. Wösten and K. Scholtmeijer, *Appl. Microbiol. Biotechnol.*, 2015, **99**, 1587–1597.
52 L. De Stefano, I. Rea, P. Giardina, A. Armenante and I. Rendina, *Adv. Mater.*, 2008, **20**, 1529–1533.
53 V. Aimanianda, J. Bayry, S. Bozza, O. Kniemeyer, K. Perruccio, S. R. Elluru, C. Clavaud, S. Paris, A. A. Brakhage, S. V. Kaveri, L. Romani and J.-P. Latgé, *Nature*, 2009, **460**, 1117–1121.
54 A. M. Gravagnuolo, S. Longobardi, A. Luchini, M.-S. Appavou, L. De Stefano, E. Notomista, L. Paduano and P. Giardina, *Biomacromolecules*, 2016, **17**, 954–964.
55 The UniProt Consortium, *Nucleic Acids Res.*, 2014, **42**, D191–D198.
56 Z. Gu, P. De Luna, Z. Yang and R. Zhou, *Phys. Chem. Chem. Phys.*, 2017, **19**, 3039–3045.
57 J. Capelo, M. Galesio, G. Felisberto, C. Vaz and J. Pessoa, *Talanta*, 2005, **66**, 1272–1280.
58 M. Lotya, Y. Hernandez, P. J. King, R. J. Smith, V. Nicolosi, L. S. Karlsson, F. M. Blighe, S. De, W. Zhiming, I. T. McGovern, G. S. Duesberg and J. N. Coleman, *J. Am. Chem. Soc.*, 2009, **131**, 3611–3620.
59 R. J. Smith, M. Lotya and J. N. Coleman, *New J. Phys.*, 2010, **12**, 125008.
60 A. G. Hsieh, S. Korkut, C. Punckt and I. a. Aksay, *Langmuir*, 2013, **29**, 14831–14838.
61 S. Wilhelm, A. J. Tavares, Q. Dai, S. Ohta, J. Audet, H. F. Dvorak and W. C. W. Chan, *Nat. Rev. Mater.*, 2016, **1**, 16014.
62 M. Lotya, A. Rakovich, J. F. Donegan and J. N. Coleman, *Nanotechnology*, 2013, **24**, 265703.
63 F. Gesuele, C. X. Pang, G. Leblond, S. Blaize, A. Bruyant, P. Royer, R. Deturche, P. Maddalena and G. Lerondel, *Phys. E*, 2009, **41**, 1130–1134.
64 U. Coscia, G. Ambrosone, F. Gesuele, V. Grossi, V. Parisi, S. Schutzmann and D. K. Basa, *Appl. Surf. Sci.*, 2007, **254**, 984–988.
65 H. Li, Q. Zhang, C. C. R. Yap, B. K. Tay, T. H. T. Edwin, A. Olivier and D. Baillargeat, *Adv. Funct. Mater.*, 2012, **22**, 1385–1390.
66 J. Kang, J.-W. T. Seo, D. Alducin, A. Ponce, M. J. Yacaman and M. C. Hersam, *Nat. Commun.*, 2014, **5**, 5478.
67 K. Kouroupis-Agalou, A. Liscio, E. Treossi, L. Ortolani, V. Morandi, N. M. Pugno and V. Palermo, *Nanoscale*, 2014, **6**, 5926–5933.

68 C. Backes, B. M. Szydłowska, A. Harvey, S. Yuan, V. Vega-Mayoral, B. R. Davies, P. Zhao, D. Hanlon, E. J. G. Santos, M. I. Katsnelson, W. J. Blau, C. Gadermaier and J. N. Coleman, *ACS Nano*, 2016, **10**, 1589–1601.
69 C. Lee, H. Yan, L. E. Brus, T. F. Heinz, J. Hone and S. Ryu, *ACS Nano*, 2010, **4**, 2695–2700.
70 X. Zhang, X.-F. Qiao, W. Shi, J.-B. Wu, D.-S. Jiang and P.-H. Tan, *Chem. Soc. Rev.*, 2015, **44**, 2757–2785.
71 Y. Guo, D. Sun, B. Ouyang, A. Raja, J. Song, T. F. Heinz and L. E. Brus, *Nano Lett.*, 2015, **15**, 5081–5088.
72 Y. Zhao, X. Luo, H. Li, J. Zhang, P. T. Araujo, C. K. Gan, J. Wu, H. Zhang, S. Y. Quek, M. S. Dresselhaus and Q. Xiong, *Nano Lett.*, 2013, **13**, 1007–1015.
73 H. M. Oh, G. H. Han, H. Kim, J. J. Bae, M. S. Jeong and Y. H. Lee, *ACS Nano*, 2016, **10**, 5230–5236.
74 X. Zhang, Z. Lai, C. Tan and H. Zhang, *Angew. Chem., Int. Ed.*, 2016, **55**, 8816–8838.
75 K. Kalantar-zadeh, J. Z. Ou, T. Daeneke, M. S. Strano, M. Pumera and S. L. Gras, *Adv. Funct. Mater.*, 2015, **25**, 5086–5099.
76 X. Gan, H. Zhao and X. Quan, *Biosens. Bioelectron.*, 2017, **89**, 56–71.
77 N. A. Kumar, M. A. Dar, R. Gul and J.-B. Baek, *Mater. Today*, 2015, **18**, 286–298.
78 G. Fiori, F. Bonaccorso, G. Iannaccone, T. Palacios, D. Neumaier, A. Seabaugh, S. K. Banerjee and L. Colombo, *Nat. Nanotechnol.*, 2014, **9**, 768–779.
79 B. Radisavljevic, A. Radenovic, J. Brivio, V. Giacometti and A. Kis, *Nat. Nanotechnol.*, 2011, **6**, 147–150.
80 D. Sarkar, W. Liu, X. Xie, A. C. Anselmo, S. Mitragotri and K. Banerjee, *ACS Nano*, 2014, **8**, 3992–4003.
81 L. Wang, Y. Wang, J. I. Wong, T. Palacios, J. Kong and H. Y. Yang, *Small*, 2014, **10**, 1101–1105.
82 C. H. Naylor, N. J. Kybert, C. Schneier, J. Xi, G. Romero, J. G. Saven, R. Liu and A. T. C. Johnson, *ACS Nano*, 2016, **10**, 6173–6179.
83 A. Azcatl, X. Qin, A. Prakash, C. Zhang, L. Cheng, Q. Wang, N. Lu, M. J. Kim, J. Kim, K. Cho, R. Addou, C. L. Hinkle, J. Appenzeller and R. M. Wallace, *Nano Lett.*, 2016, **16**, 5437–5443.
84 D. Pierucci, H. Henck, Z. Ben Aziza, C. H. Naylor, A. Balan, J. E. Rault, M. G. Silly, Y. J. Dappe, F. Bertran, P. Le Fèvre, F. Sirotti, A. T. C. Johnson and A. Ouerghi, *ACS Nano*, 2017, **11**, 1755–1761.
85 W. S. Leong, Y. Li, X. Luo, C. T. Nai, S. Y. Quek and J. T. L. Thong, *Nanoscale*, 2015, **7**, 10823–10831.
86 Z. Wang, W. Zhu, Y. Qiu, X. Yi, A. von dem Bussche, A. Kane, H. Gao, K. Koski and R. Hurt, *Chem. Soc. Rev.*, 2016, **45**, 1750–1780.